Hetero-Integrated InP RTD-SiGe BiCMOS Source With Fundamental Injection Locking

E. Mutlu, *Member, IEEE*, C. Preuss, *Graduate Student Member, IEEE*, F. Vogelsang, *Graduate Student Member, IEEE*, R. Kress, *Member, IEEE*, J. Bott, *Member, IEEE*, B. Sievert, *Member, IEEE*, J. Watermann, J. Abts, A. Rennings, *Member, IEEE*, D. Erni, *Member, IEEE*, N. Pohl, *Senior Member, IEEE*, and N. Weimann, *Member, IEEE*

***Abstract*— This work shows the hetero-integration of an InP resonant tunneling diode (RTD) on a SiGe-BiCMOS mm-Wave integrated circuit (MMIC) for near-field wireless fundamental injection locking. We observe injection locking within a locking range of 26 GHz and a total power during injection locking of −3.4 dBm. The SiGe-based local oscillator (LO) is integrated with a frequency doubler and an on-chip patch antenna that operates between 220 and 247 GHz, providing a maximum output power of −7 dBm. The LO is near-field coupled to an InP RTD oscillator integrated into a slot antenna which reaches a free running maximum output power of −6.2 dBm. The chip-to-chip integration is carried out through flip-chip bonding.**

***Index Terms*— BiCMOS, flip-chip bonding, hetero-integration, indium phosphide (InP), injection locking, mm-Wave, mm-Wave integrated circuit, monolithic microwave integrated circuit (MMIC), resonant tunneling diode (RTD), silicon-germanium (SiGe), THz.**

I. INTRODUCTION

RESONANT tunneling diode (RTD) oscillators based on indium phosphide (InP) have been shown to exhibit oscillation close to 2 THz [1], and the application of these very compact devices in diverse scenarios such as wireless broadband links, nondestructive quality control and characterization of plants [2], [3], [4], [5], [6] could be demonstrated. An integrated oscillator circuit is formed when monolithically integrating the RTD into an antenna [7]. Spatial combination in an array was demonstrated with 6 × 6 InP RTD elements emitting more than 10 mW at 450 GHz [8]. In real-time mobile applications, electronic beam steering of radiation emanating the array would be beneficial [9], requiring precise phase control of individual pixels, which can be achieved through injection locking [10].

The concept of wireless injection locking and thus control of the phase of InP RTD oscillators with fundamental and subharmonic injection signals could already be proven in early experiments [11], [12], [13]. The subharmonic injection locking process multiplies the controlling frequency, which is convenient in the THz range, where transistor-based control circuits only reach limited operating frequencies. In recent publications of injection-locked InP RTD THz sources, external instruments (THz extenders) were used as a locking source. Real-world applications require integrated sources, combining both the THz oscillator and locking signal generation into a single integrated module, to facilitate the development of mobile, lightweight systems. In this letter, we demonstrate a compact hetero-integrated device consisting of an InP RTD oscillator flip-chip-bonded on top of a free running SiGe-local oscillator (LO) mm-Wave integrated circuit (MMIC) (see Section II) exhibiting injection locking (see Section III). The corresponding concept sketch is shown in Fig. 1. The LO signal generator is realized in BiCMOS technology as an injection source that offers high bandwidth and power in the WR3.4 band [14]. For optimum performance, subharmonic injection locking via a radiative control signal requires a two-band antenna fit to the RTD. Here, we use fundamental injection locking for simplicity and forgo the use of a dual-band antenna, similar to designs presented in [15].

II. DESIGN AND FABRICATION

A. InP RTD Oscillator

According to Adler [16], phase and frequency deviation of a locked oscillator from the injection source are described in steady state by

$$\frac{\Delta\omega_0}{\omega_0} = \frac{1}{2Q}\sqrt{\frac{P_{\text{inj}}}{P_0}}\sin(\Delta\phi) \quad (1)$$

Received 24 July 2024; accepted 7 September 2024. Date of publication 30 September 2024; date of current version 8 November 2024. This work was supported in part by the Deutsche Forschungsgemeinschaft Sonderforschungsbereich (SFB)/Transregio (TRR) 196 MARIE, Subproject C02, C03, and C05, under Project 287022738; in part by the Research Network Terahertz North Rhine-Westphalia (NRW) within the Program "Netzwerke 2021," an initiative of the Ministry of Culture and Science of the State of NRW under Grant NW21-068C; in part by German Federal Ministry of Education and Research (BMBF) in the course of 6G Research Hub "6GEM" within the German Federal Government Program "Research and Innovation 2016–2020" under Grant 16KISK039; and in part by the State of NRW within the EFRE 2014–2020 Framework "Investment in Growth and Employment" through the Project "Terahertz-Integrationszentrum (THzIZ), under Grant EFRE0400215." *(Corresponding author: E. Mutlu.)*

E. Mutlu, C. Preuss, R. Kress, J. Watermann, J. Abts, and N. Weimann are with the Department of Components for High Frequency Electronics (BHE), Faculty of Engineering, University of Duisburg-Essen, D-47057 Duisburg, Germany, and also with the Center for Nanointegration Duisburg-Essen (CENIDE), D-47048 Duisburg, Germany (e-mail: enes.mutlu@uni-due.de).

F. Vogelsang and J. Bott are with the Institute of Integrated Systems, Ruhr-Universität Bochum, D-44801 Bochum, Germany.

B. Sievert is with the Fraunhofer Institute for High Frequency Physics and Radar Techniques FHR, D-53343 Wachtberg, Germany.

A. Rennings and D. Erni are with the Laboratory for General and Theoretical Electrical Engineering (ATE), Faculty of Engineering, University of Duisburg-Essen, D-47057 Duisburg, Germany, and also with the Center for Nanointegration Duisburg-Essen (CENIDE), D-47048 Duisburg, Germany.

N. Pohl is with the Institute of Integrated Systems, Ruhr-Universität Bochum, D-44801 Bochum, Germany, and also with the Fraunhofer Institute for High Frequency Physics and Radar Techniques FHR, D-53343 Wachtberg, Germany.

Color versions of one or more figures in this letter are available at https://doi.org/10.1109/LMWT.2024.3458196.

Digital Object Identifier 10.1109/LMWT.2024.3458196

© 2024 The Authors. This work is licensed under a Creative Commons Attribution-NonCommercial-NoDerivatives 4.0 License. For more information, see https://creativecommons.org/licenses/by-nc-nd/4.0/

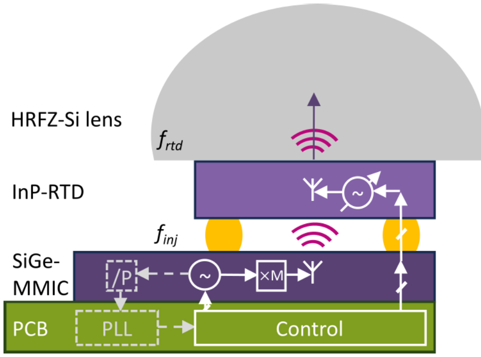

Fig. 1. Schematic sketch of the hetero-integrated module.

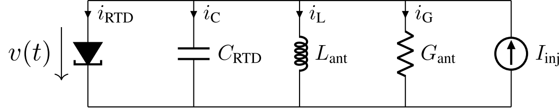

Fig. 2. Simple equivalent circuit of an InP RTD oscillator with an injected signal represented by a current source I_{inj} [10].

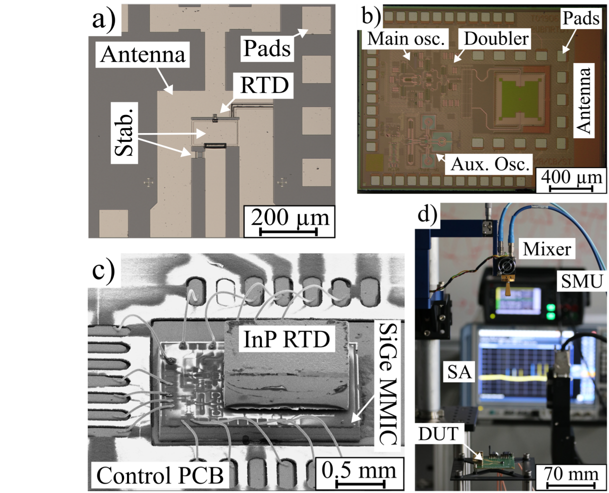

Fig. 3. Micrograph of (a) InP RTD oscillator, (b) BiCMOS MMIC, and (c) integrated InP/SiGe stack before lens integration. The measurement setup is shown in (d).

with the free running angular frequency ω_0, the angular frequency change due to the injection signal $\Delta\omega_0$, injected power P_{inj}, power of the free running oscillator P_0, the oscillator's quality factor Q and the phase difference $\Delta\phi$ between injected and emitted signal. Adler's equation can be used to estimate the locking range, which determines the available instantaneous bandwidth of the injection-locked RTD, and sets limits to the maximum phase tunability in phased array beam steering related to $\Delta\phi$. The maximum locking range depends not only on the ratio of injected and emitted power but also on the quality factor. The equivalent circuit of the RTD oscillator during injection locking is shown in Fig. 2 as a simplified circuit. Applying Kirchhoff's first law and nonlinear analysis of this circuit results in an equation in the form of a Van der Pol oscillator [17]

$$\ddot{x} + \epsilon\left(x^2 - 1\right)\dot{x} + x = I_{inj}. \tag{2}$$

In this second-order differential equation, the nonlinearity factor ϵ is introduced, depending on the total conductance G, antenna inductance L_{ant}, and RTD capacitance C_{RTD} as follows:

$$\epsilon = G\sqrt{\frac{L_{ant}}{C_{RTD}}}. \tag{3}$$

For a parallel RLC resonator, $Q = R\sqrt{C/L}$, which is the inverse of ϵ [18]. The relationship between Q and ϵ implies that increased nonlinearity in oscillators substantially expands the locking range according to (1) [10]. Therefore, a stronger nonlinearity is preferred in the oscillator design.

The RTD oscillator chip is realized by monolithic integration of a double-barrier RTD into a slot antenna with a slot length of 166 μm and a slot width of 9 μm. The RTD layer stack is grown by molecular beam epitaxy on a semi-insulating InP (100) substrate. Fabrication of the device is carried out in top-down processing using standard optical lithography, wet and dry etching techniques, and metal lift-off. Further details on layer stack and technology process are given in [19] and [20]. The employed layer stack exhibits a peak current density of 12 mA/μm^2 at 0.31 V. A stabilization resistor of nominally 10 Ω is formed in the n$^+$-InGaAs mesa. Plasma-enhanced chemical vapor deposited SiN is employed as a dielectric material in a metal-insulator–metal (MIM) capacitor, splitting the dc and RF paths of the oscillator. A slot-type antenna is chosen here because of its linearly polarized radiation through the substrate. The polarity aligns with the emission of the injection source. This allows injection from the surface side of the InP chip while the primary emission is transmitted through the substrate. The fabricated oscillator is depicted in Fig. 3(a). The antenna's impedance is complex conjugate impedance matched to the InP RTD. A radiation efficiency of 56 % was extracted from 3-D electromagnetic field simulation (Empire XPU). The RTD's small cross-sectional area of 0.6 μm^2 results in low device capacitance. As a result, when the oscillator is subjected to a large antenna inductance, it exhibits significant nonlinearity, as indicated by (3). The value of ϵ, as defined in (3), is approximately 0.8.

B. SiGe-BiCMOS MMIC

The SiGe MMIC provides a stabilized injection locking signal at the fundamental frequency of the RTD. The SiGe circuits are based on [21] and were realized in Infineon's B11HFC SiGe BiCMOS technology [22]. To generate the signal, a VCO operating at a subharmonic frequency of 120 GHz is implemented in Colpitts architecture. Following the VCO, a push-push frequency doubler generates a high-power output signal, resulting in an output frequency of 240 GHz. An on-chip patch antenna [21] is used for near-field coupling of the SiGe chip's output signal to the RTD. The pad frame supports flip-chip mounting of the RTD chip and provides dc bias feedthrough. For frequency stabilization, an offset phase-locked loop (PLL) is included. An additional auxiliary VCO at 34 GHz with its own static frequency divider drives an offset mixer. With this mixed output, an off-chip PLL setup can be used to generate an output signal stabilized to an external reference. Fig. 3(b) shows the manufactured MMIC where the key elements are highlighted.

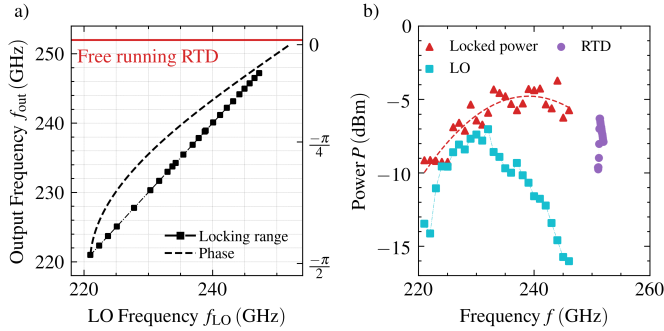

Fig. 4. Measured locked frequency versus. LO frequency, and resulting phase shift of InP RTD, according to (1) (a). Extracted locked power compared to the available power of the individual components (b).

C. Hetero-Integration Design and Process

The design of the hetero-integrated component includes all functions for frequency-controlled THz generation and only needs external bias sources. The design is scalable to many pixels. Phase control can be easily added by $C(V)$ tuning of the RTD (1) and within the SiGe LO. A PCB made from low-cost FR-4 serves as a chip carrier and control unit. For hetero-integration, first, gold bumps for the SiGe-InP flip-chip interconnect are placed onto the SiGe MMIC by forming balls from bond wire in an F&S Bondtech (53xxBDA) wire bonder. Thirteen gold bumps are placed onto the pads close to the patch antenna [see Fig. 3(b)]. Only two pads are needed for electrical control of the InP RTD. The additional bumps provide for mechanical stability during the flip-chip bonding process. Then, the SiGe chip is mounted onto the PCB, affixed with thermoconductive silver paste, and electrically connected to the board using wedge-to-wedge wire bonds. Subsequently, the InP RTD chip is flip-chip mounted onto the SiGe chip using thermocompression with 60 g/bump force at 120 °C and 300 °C at board and chip, respectively, in a precision chip aligner (Fineplacer sigma, finetech). For good near-field coupling, the electric field orientation of both antennas should be in parallel. After compression, the height and diameter of the bumps amount to 54 and 75 μm, respectively. The completed InP/SiGe/RF board stack including wire bonds is shown in the scanning electron microscope image of Fig. 3(c). The backside of the InP chip faces upward, and the THz radiation of the integrated slot antenna emanates from this surface. To enhance the outcoupling efficiency from the InP substrate, a hyper-hemispherical lens made from high-resistive float zone silicon with 5 mm diameter and 2.9 mm thickness is attached. The axis of the Si lens is carefully aligned to the slot antenna, and fixed in place in an adhesive bonding step employing an UV cured adhesive in the same chip aligner.

III. Injection Locking Experiment

The functionality of the hetero-integrated module is verified in an injection locking experiment. The module's output signal is recorded in a far-field setup shown in Fig. 3(d), which includes a motorized stage for positioning of the module. A heterodyne mixer module operating in the WR3.4 band (WR3.4MixAMC, VDI) is used to downconvert the signal, and the mixing product is recorded with a phase noise analyzer in spectrum analysis mode (FSWP50, R&S). During the locking experiment, we operated the RTD oscillator at a fixed bias of 0.63 V—resulting in free running oscillation at 252 GHz—and we swept the SiGe-LO frequency between 220 GHz and 247 GHz, as shown in Fig. 4(a). Locking is observed over nearly the full frequency range of the SiGe MMIC, starting at 221 GHz. On the right axis, the extracted phase change according to (1) is also depicted. Since the RTD's free running oscillation is above the tuning range of the LO, we could only observe the lower half of the locking range. In addition, the SiGe-LO and InP RTD were individually measured without locking to assess their individual performance, as presented in Fig. 4(b). In the quasioptic setup, we measured an individual maximum output power of −7 and −6.2 dBm for the individual SiGe-LO and InP RTD, respectively, removing the free space path loss according to Friis' formula. The maximum injected power $P_{\text{inj,max}}$ amounts to −17 dBm, accounting for a coupling loss of 10 dB. A significant increase in total power during locked conditions is observable. In the upper tuning range of the LO, the SiGe LO's output power weakens, while in locked conditions, a much higher amount of total power is recorded, which is contributed by the locked RTD. The observed locking range is 26 GHz. However, we could not evaluate the upper end of the locking range due to the limited bandwidth of the SiGe LO chip. A comparison of our results with injection locking experiments of RTDs published in literature is shown in Table I.

TABLE I
Comparison of Injection Locked RTD Oscillators

f_0 (GHz)	Locking type	Locking source	P_{inj} (dBm)	P_0 (dBm)	Δf_{lock} (GHz)	Ref.
550	$f_0/2$	Signal gen.	0§	-18	2	[12]*
383	f_0	Signal gen.	-25.1	-25.2	2	[13]*
322	f_0	UTC-PD	-27	-21	0.5	[23]*
338	f_0	Ti:Al_2O_3 laser	-	-	10	[24]*
252	f_0	SiGe-MMIC	-17	-6.2	26	**This work.**†

*External locking signal, †Fully integrated, §Signal generators output.

IV. Conclusion

We presented the proof-of-concept for a highly compact THz source consisting of an InP RTD oscillator and a SiGe BiCMOS injection locking source. The InP and BiCMOS chips were hetero-integrated in a thermocompression flip-chip bonding process. The assembled stack was mounted on a control PCB, and a Si lens was added for enhanced radiation outcoupling. The integrated component could be demonstrated to operate under fundamental injection locking from 221 to 247 GHz exhibiting a tuning range of 26 GHz.

References

[1] R. Izumi, S. Suzuki, and M. Asada, "1.98 THz resonant-tunneling-diode oscillator with reduced conduction loss by thick antenna electrode," in *Proc. 42nd Int. Conf. Infr., Millim., THz Waves (IRMMW-THz)*, Aug. 2017, pp. 1–2.

[2] A. Oshiro et al., "PAM4 48-Gbit/s wireless communication using a resonant tunneling diode in the 300-GHz band," *IEICE Electron. Exp.*, vol. 19, no. 2, Jan. 2022, Art. no. 20210494.

[3] X. Yu, R. Yamada, J.-Y. Kim, M. Fujita, and T. Nagatsuma, "Integrated circuits using photonic-crystal slab waveguides and resonant tunneling diodes for terahertz communication," in *Proc. Prog. Electromagn. Res. Symp. (PIERS-Toyama)*, Toyama, Japan, Aug. 2018, pp. 599–605.

[4] T. Miyamoto, A. Yamaguchi, and T. Mukai, "Terahertz imaging system with resonant tunneling diodes," *Jpn. J. Appl. Phys.*, vol. 55, no. 3, Jan. 2016, Art. no. 032201.

[5] F. Sheikh et al., "Towards continuous real-time plant and insect monitoring by miniaturized THz systems," *IEEE J. Microw.*, vol. 3, no. 3, pp. 913–937, Jul. 2023.

[6] M. Gezimati and G. Singh, "Terahertz imaging and sensing for healthcare: Current status and future perspectives," *IEEE Access*, vol. 11, pp. 18590–18619, 2023.

[7] M. Asada, S. Suzuki, and N. Kishimoto, "Resonant tunneling diodes for sub-terahertz and terahertz oscillators," *Jpn. J. Appl. Phys.*, vol. 47, no. 6R, p. 4375, Jun. 2008.

[8] Y. Koyama et al., "A high-power terahertz source over 10 mW at 0.45 THz using an active antenna array with integrated patch antennas and resonant-tunneling diodes," *IEEE Trans. THz Sci. Technol.*, vol. 12, no. 5, pp. 510–519, Sep. 2022.

[9] Y. Monnai, X. Lu, and K. Sengupta, "Terahertz beam steering: From fundamentals to applications," *J. Infr., Millim., THz Waves*, vol. 44, nos. 3–4, pp. 169–211, Apr. 2023.

[10] M. Asada, "Theoretical analysis of subharmonic injection locking in resonant-tunneling-diode terahertz oscillators," *Japanese J. Appl. Phys.*, vol. 59, no. 1, Jan. 2020, Art. no. 018001.

[11] K. Arzi, G. Keller, A. Rennings, D. Erni, F.-J. Tegude, and W. Prost, "Frequency locking of a free running resonant tunneling diode oscillator by wire-less sub-harmonic injection locking," in *Proc. 10th U.K.-Eur.-China Workshop Millimetre Waves THz Technol. (UCMMT)*, Sep. 2017, pp. 1–4.

[12] K. Arzi et al., "Subharmonic injection locking for phase and frequency control of RTD-based THz oscillator," *IEEE Trans. Terahertz Sci. Technol.*, vol. 10, no. 2, pp. 221–224, Mar. 2020.

[13] Y. Suzuki, T. Van Mai, X. Yu, S. Suzuki, and M. Asada, "Phase control of terahertz waves using injection-locked resonant tunneling diode oscillator," *IEEE Trans. THz Sci. Technol.*, vol. 12, no. 5, pp. 481–488, Sep. 2022.

[14] D. Kissinger, G. Kahmen, and R. Weigel, "Millimeter-wave and terahertz transceivers in SiGe BiCMOS technologies," *IEEE Trans. Microw. Theory Techn.*, vol. 69, no. 10, pp. 4541–4560, Oct. 2021.

[15] M. Zhang et al., "Antenna design for subharmonic injection-locked triple barrier RTD oscillator in the 300 GHz band," in *Proc. 2nd Int. Workshop Mobile THz Syst. (IWMTS)*, Bad Neuenahr, Germany, Jul. 2019, pp. 1–4.

[16] R. Adler, "A study of locking phenomena in oscillators," *Proc. IEEE*, vol. 61, no. 10, pp. 1380–1385, Oct. 1973.

[17] T. Hiraoka, "Nonlinear response of resonant-tunneling-diode terahertz oscillator," Ph.D. dissertation, Dept. Phys., Kyoto Univ., Kyoto, Japan, 2021.

[18] J. White, *LC Resonance and Matching Networks*. Hoboken, NJ, USA: Wiley, 2003, ch. 3, pp. 59–77.

[19] E. Mutlu et al., "Investigation of RTD THz oscillator with wide frequency tuning capability," in *Proc. 48th Int. Conf. Infr., Millim., Terahertz Waves (IRMMW-THz)*, Montreal, QC, Canada, Sep. 2023, pp. 1–2.

[20] E. Mutlu et al., "Large-signal device model verification for resonant tunneling diode oscillator," in *Proc. 6th Int. Workshop Mobile THz Syst. (IWMTS)*, Bonn, Germany, Jul. 2023, pp. 1–5.

[21] S. Thomas, C. Bredendiek, and N. Pohl, "A SiGe-based 240-GHz FMCW radar system for high-resolution measurements," *IEEE Trans. Microw. Theory Techn.*, vol. 67, no. 11, pp. 4599–4609, Nov. 2019.

[22] J. Böck et al., "SiGe HBT and BiCMOS process integration optimization within the DOTSEVEN project," in *Proc. IEEE Bipolar/BiCMOS Circuits Technol. Meeting*, Oct. 2015, pp. 121–124.

[23] T. Hiraoka et al., "Injection locking and noise reduction of resonant tunneling diode terahertz oscillator," *APL Photon.*, vol. 6, no. 2, pp. 1–7, Feb. 2021.

[24] T. Arikawa et al., "Injection locking of resonant tunneling diode oscillator using coherent terahertz pulses," in *Proc. 44th Int. Conf. Infr., Millim., THz Waves (IRMMW-THz)*, Paris, France, Sep. 2019, pp. 1–3.